JOURNAL OF PROPULSION AND POWER
Vol. 11, No. 6, November–December 1995

Laser Propulsion 10-kW Thruster Test Program Results

J. Black* and H. Krier†
Combustion Sciences, Inc., Champaign, Illinois 61821
and
R. J. Glumb‡
TRW Space and Technology Group, Redondo Beach, California 90278

This article summarizes the results of the first-ever experimental tests of a 10-kW laser-powered rocket engine. The rocket engine used high-temperature laser-sustained plasmas to heat flows of argon and hydrogen propellants, which were then exhausted through a rocket nozzle to generate thrust. The design of the thruster and test support equipment is described in detail, followed by a summary of performance data, particularly specific impulse and thruster efficiency. Specific impulse values of up to 350 s at efficiencies near 40% were obtained using hydrogen propellant. A low-velocity stability limit for laser-sustained plasmas was also discovered, which may have important implications for the design of future laser propulsion systems.

Introduction

SINCE the early 1970s, it has been known that high-power lasers could be used to generate rocket thrust for propulsion applications. The concept was first introduced by Kantrowitz,[1] who recognized that the high specific impulse capability and low structural weight of laser propulsion gives it significant advantages over other propulsion systems. For example, an operational laser thruster with specific impulse performance in the range of 1000–1500 s could greatly increase payload mass fractions in many orbital transfer mission applications, significantly reducing the costs of space transportation.

One method for efficiently converting the energy of a laser beam into the thermal energy of a propellant gas for propulsion is through the use of high-temperature laser-sustained plasmas (LSPs), as shown in Fig. 1. The LSP is a stationary region of high-temperature electrically neutral plasma that forms near the focus of a high-power laser beam. It absorbs laser energy through an inverse bremsstrahlung absorption process, which results in very high absorption fractions (usually 75–95%, with higher absorption occurring at higher laser powers and higher gas pressures). Peak temperatures within the plasma are typically 20,000–30,000 K.

By introducing a flow of propellant gas into the plasma in the same direction as that of the laser, the thermal transport of the plasma (i.e., the upstream conductive heat transfer that causes the plasma to propagate upstream) is balanced by the flow velocity of the gas. Moreover, by using a focused beam geometry, the plasma will tend to stabilize at a beam intensity location where the thermal fluxes just balance, and the plasma tends to be quite stable at that location. As propellant gas flows through and around the stationary plasma and mixes with nonheated gas, high bulk temperatures (typically 2000–4000 K) are achieved. The heated propellant gas is then exhausted through a rocket nozzle to generate thrust. Because of the high temperatures and low molecular weight of the propellant gas, specific impulse performance can be exceptionally good (in excess of 1000 s when using hydrogen propellant).

Experimental work during the 1980s characterized the stability and conversion efficiency of LSPs under a wide range of flow conditions, and for different propellant gases.[2,3] This work verified that LSPs were highly stable phenomena, which could efficiently convert laser energy into the thermal energy of a propellant gas. Two-dimensional plasma modeling predictions also indicated favorable scaling behavior at higher laser powers.

This pioneering work paved the way for an actual demonstration of a laser-powered rocket engine. In 1989, the authors began a Small Business Innovative Research (SBIR) program to design and build a laser-powered rocket engine, perform tests at 10-kW power levels, and measure thrust, specific impulse, and efficiency over a wide range of operating conditions. The hydrogen-fueled thruster was designed for specific impulse performance in the range of 300–700 s, with a planned efficiency of about 50%. This performance is only an intermediate step in the path towards developing a full-scale thruster, which would operate at specific impulse levels in excess of 1000 s and efficiencies near 90%. A more detailed program report containing additional design information and test data is also available.[4]

Laser Thruster Design

Developing a reliable design for a laser-powered rocket engine represented a significant technical challenge due to the high temperatures created by the LSP, and the extremely high laser fluxes that must be accepted by the thruster. Extensive thermal and optical simulations were used to develop the design. For example, one simulation assessed the thermal energy radiated from the plasma to the thruster walls; another calculated internal laser beam reflection patterns inside the thruster; and a third predicted temperature rises within the thruster nozzle walls during operation. A detailed LSP model was also used to predict plasma performance over the range of expected operating conditions. Using these models, the key design characteristics of the thruster (throat geometry, laser focal length, window size, operating pressure, and nominal location of the plasma) were traded until an optimal design was achieved.

Figure 2 is a schematic diagram of the final thruster configuration developed for the 10-kW tests. The thruster is cylindrical in shape, with the laser beam entering from below through a zinc selenide window. This vertical orientation was used to compensate for fluid buoyancy effects that arise when

Received July 1, 1994; revision received Dec. 26, 1994; accepted for publication Dec. 28, 1994.

*Chief Engineer, 208 Elmwood Road.
†President and Chief Scientist, 208 Elmwood Road. Fellow AIAA.
‡Section Head, O1/1020, One Space Park. Senior Member AIAA.

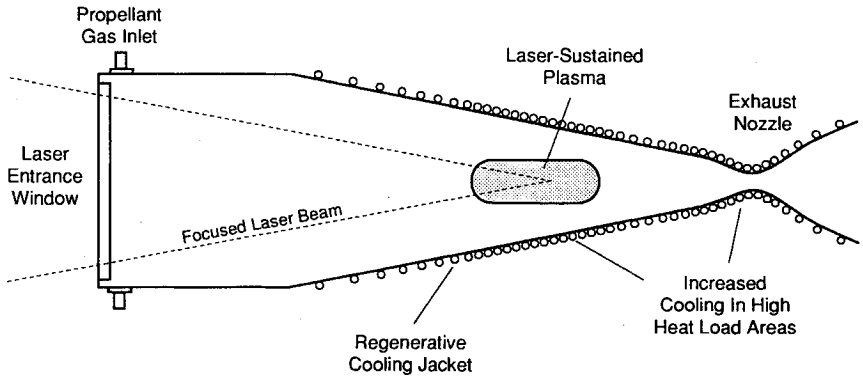

Fig. 1 Conceptual design for a laser-powered rocket engine using laser-sustained plasmas.

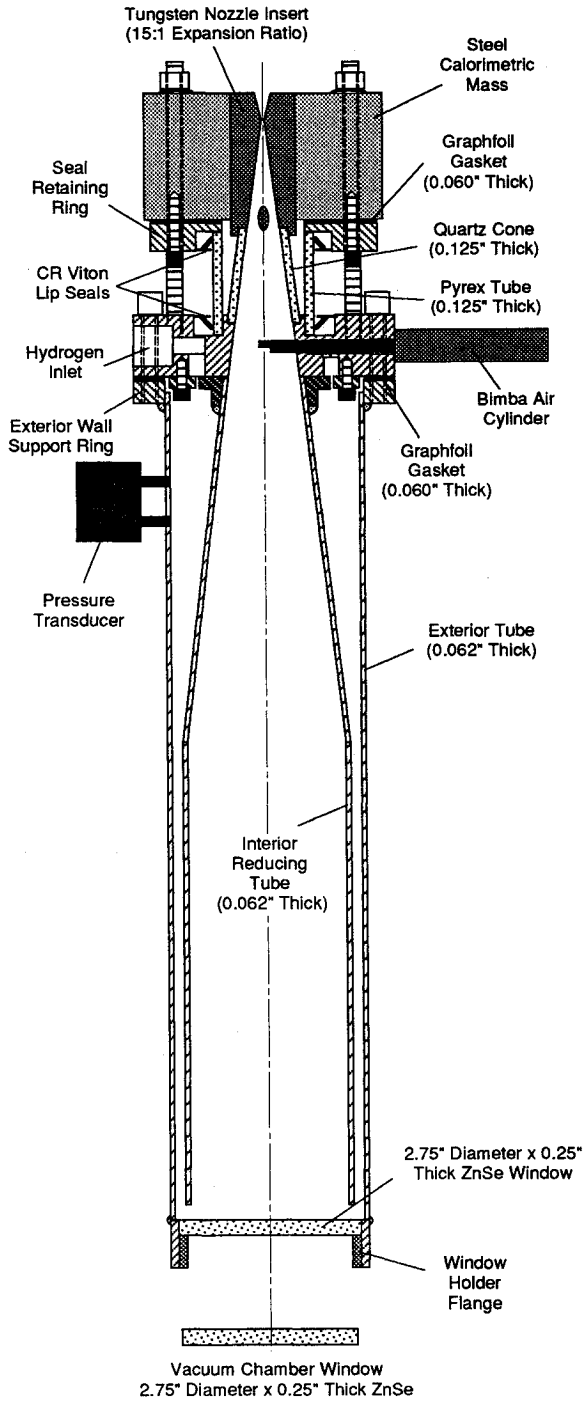

Fig. 2 Design drawing for the 10-kW laser thruster unit.

the propellant gas is heated. The beam is focused to a point just below the throat section of the thruster, where the high-temperature LSP is stabilized. The propellant gas enters the thruster near its midsection, and flows down through an annular region to the bottom of the thruster, where it is used to cool the laser inlet window. The flow is then directed upwards, flows through and around the plasma, and is exhausted out the nozzle section at the top. The nominal operating pressure of the thruster is 2.0 atm, but any intermediate pressure from 0 to 5 atm can be used.

The most critical portion of the thruster is the throat region; an enlarged sketch of this area is shown in Fig. 3. A key requirement is that the plasma must be stabilized at a location where the flow velocity at the plasma front maximizes the plasma efficiency (5–8 m/s at 2.0 atm), but does not exceed the blowout velocity of the plasma (about 20 m/s). An important advantage of the selected conical geometry is that the flow velocity at the plasma can be changed simply by making small adjustments in the vertical location of the plasma (achieved through small movements of a motorized focusing lens). In this way, different plasma operating conditions can be studied to identify high-efficiency conditions.

Selection of the laser optics focal ratio (i.e., the focal length divided by the beam diameter) also impacted the throat section design. Moderate f numbers (between $f/5$ and $f/9$) are desirable for maximum plasma stability and efficiency (plasmas tend to become unstable at higher values, and suffer efficiency penalties at lower values). However, care must be taken to avoid laser damage of the throat walls (since as much as 40% of the incident beam can be transmitted through the plasma). To avoid this, the diameter and convergence angle of the throat section must be carefully selected. The throat can either be designed so that the transmitted beam passes cleanly through the throat as shown in Fig. 3 (this requires high f numbers and a steeply converging wall angle), or the beam can be intentionally made to reflect off the walls prior to passage out the throat (which requires shorter optical f numbers and a more shallow wall angle). These two operating modes are known as "through-the-throat" and "single-bounce"operations, respectively.

In the end, a relatively high $f/8.5$ system was selected due to its flexibility in operating with the six different throat configurations that were chosen to allow studies over a wide range of operating conditions (including the use of different propellant gases). Two throats were designed for checkout tests using argon propellant. These were constructed with large 5.0-mm i.d. throats and two different wall angles (19 and 8 deg) to demonstrate either through-the-throat or single-bounce operation. The large throat sizes keep propellant temperatures low, minimizing risks of thermal damage, but resulting in low performance. Because of the low propellant temperatures, both of these throats were made of copper. Two 19-deg throat sections were designed for hydrogen operation, and used tungsten construction with throat diameters of 2.0

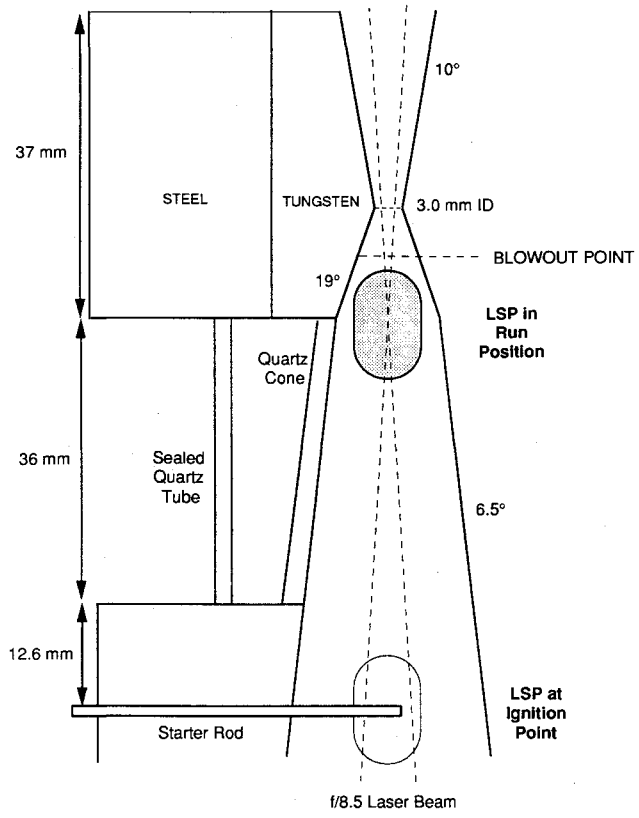

Fig. 3 Close-up of thruster throat section identifying key design geometry considerations.

and 3.0 mm. The 2.0-mm throat was designed for high specific impulse performance. The 3.0-mm throat was intended to be used during early hydrogen tests, and for some argon tests. The two final nozzle throat geometries used a much shallower wall angle (6.5 deg) to assess the effects of single-bounce operation on efficiency and specific impulse. These nozzles were built with 2.0- and 1.75-mm i.d. throats, and were made from tungsten.

Directly below the throat section is a small conical quartz viewing window that is used to view and photograph the plasma. The inclusion of this feature required considerable design work due to the high thermal loads in the vicinity of the plasma. Quartz was selected since most of the radiation emitted by the plasma is in visible and near-IR wavelengths, which the quartz will transmit. A combination of a nonpressurized inner cone and a sealed outer quartz tube was used, with sealing provided by radial lip seals. This design proved to be highly successful, and no quartz section failures were experienced.

The final design of the throat sections consisted of an inner machined throat insert (made of either copper or tungsten), and an outer steel section that was used as a heat sink to absorb the thermal energy produced by the thruster during its nominal 2-min operating period. Figure 4 is a photograph of the upper portion of the thruster, showing the nozzle insert with outer steel heat sink, the quartz viewing section, and a "starter block" assembly containing a pneumatic cylinder for starter rod insertion. A key feature of this design was that it allowed the throat sections to be interchanged quickly and easily.

Although the plasma is located at the position indicated in Fig. 3 during operation, the plasma must first be initiated. This is needed because the cold gas is transparent to the IR energy of the CO_2 laser beam, and some method is needed to initially raise the temperature of the gas so that it can begin absorbing. Many different techniques have been used in the past to start plasmas (electric arcs, pulsed laser beams, and

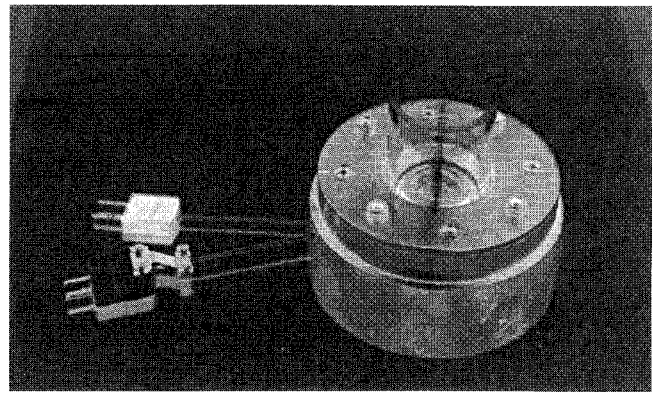

Fig. 4 Photograph of thruster throat section, quartz viewing section, and starter block containing tungsten rod for plasma initiation.

seeded gases), but we have used what has proven to be a very reliable approach: the momentary insertion of a tungsten rod into the laser beam focus point.[2]

In our design, plasmas are initiated by first moving the focus point downwards to the height of a tungsten "starter rod." The rod is momentarily inserted into the laser focus point, where the intense surface heating releases free electrons into the gas above the rod, and the gas begins absorbing laser energy through an inverse bremsstrahlung process. Once the gas becomes hotter and reaches a self-sustaining level, the rod is removed to prevent damage. The focus point is then moved back upwards to its normal run position, with the plasma stably following the upward motion of the focus point. A double-acting pneumatic cylinder was used to actuate the starter rod. This approach has the advantages of compact size, high force levels in both directions independent of stroke position, a long stroke length, and easy sealing capabilities.

Test Support Equipment Design

A number of unique test support systems were developed for the 10-kW thruster tests. The first was a thrust stand to support the thruster during operation, while allowing highly accurate thrust measurements to be made. The thrust measurement system was constrained by the requirements that the thruster be aligned vertically (to minimize plasma buoyancy effects), and that the motion of the thruster during operation be minimized to avoid disturbing the alignment of the laser-focusing optics. After a number of options were considered,[4] the final configuration shown in Fig. 5 was chosen.

The thrust stand linkage consists of a counterbalanced pulley centered around a low-friction Lucas free-flex pivot; the thruster hangs from one side of the pivot and a large counterweight is hung from the other side. Two parallel sheet metal flexures are also mounted to the thruster and the counterweight sides of the balance to prevent any horizontal swinging of the thruster or counterweight. This arrangement results in very low frictional resistance to motions produced by thrust outputs, and because the supporting wire is always located at the same radius from the pulley pivot center, no significant horizontal deflections occur even at relatively large vertical displacements.

To measure the thrust output, a combination of a linear variable differential transformer (LVDT) and an active electromagnetic "counterforce coil" was used. In operation, the LVDT senses any motion of the thruster caused by thrust output, and the magnetic coil is then energized to keep the thruster located at a nominal null-displacement position. The electrical current supplied to this coil is then accurately calibrated to read out as the thrust level being produced by the engine. Small counterweights are dropped onto the counterweight side of the balance before and after each test to ac-

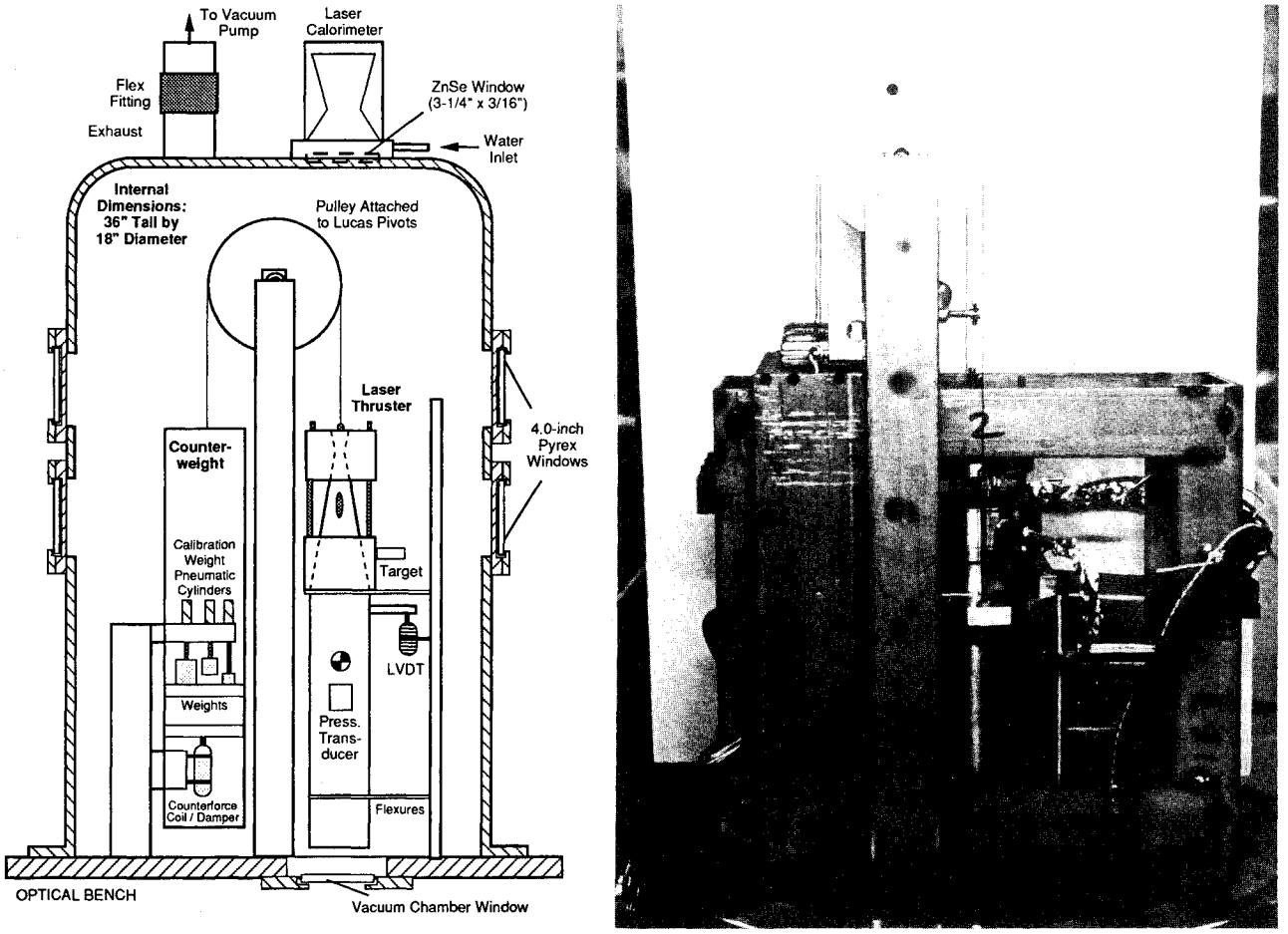

Fig. 5 Design drawing (left) and photograph (right) of thruster mounted in thrust measurement linkage assembly.

curately calibrate the system. The counterforce coil also fulfills the function of absorbing any vibratory energy from the thruster that could cause the counterweighted balance to oscillate. This system represents a major improvement over similar types of thrust measurement devices currently available, and performed flawlessly throughout the tests.

The thruster and thrust stand were mounted to the test stand shown in Fig. 6. The test stand included a Newport vibration-isolation table, a vacuum bell jar to maintain the thruster in vacuum during operation, and a series of laser optics that is used to focus the laser beam inside the thruster. A water-cooled calorimeter was also mounted to the top of the bell jar to monitor laser energy leaving the thruster.

The laser-focusing optics consisted of two water-cooled copper flat mirrors that accepted a horizontal beam from the 10-kW laser, and redirected it upwards into a 10.16-cm diam *f*/8.5 ZnSe lens, which then focused the beam inside the thruster. The input laser beam at the lens entrance was annular in shape (resembling a TEM-01* mode shape), with a 5.8 cm i.d. and a 7.6 cm o.d.. Both mirrors used precision gimbal mounts to allow very accurate positioning of the beam inside the thruster. The focusing lens was attached to a stepper-motor drive controlled remotely by the experiment control computer. Movements of the lens allowed the plasma location to be shifted relative to the throat during each test.

The entire thruster assembly was housed in an evacuated bell jar maintained at about 30 torr during thruster operation. Eight radial vacuum feed-throughs were used to route electrical wires and propellant feed lines into the bell jar. The top of the bell jar emptied into a 10-cm diam exhaust duct, connected to two 70-l/s vacuum pumps in an adjacent room. Flexible stainless-steel bellows, rubber isolation sleeves, and spring-loaded ceiling hangers were successfully used to prevent pump vibrations from being transmitted back to the thrust measurement system.

A Macintosh-based computer system was used to collect all critical thruster data, while ensuring safe operations by monitoring and controlling most aspects of the tests. This system continuously monitored pressures and temperatures within the thruster, vacuum pressures, propellant flow rates, laser output power, and a series of hydrogen leak detectors located throughout the lab. In the event of an anomaly, the computer either alerted the operator (for minor anomalies), or initiated a complete shutdown of the experiment including disabling the laser and initiating an argon purge flow through the thruster.

The computer system was also used to control the time-critical plasma-initiation process. After the initiation procedure was initiated by the operator and the laser power was ramped up, the computer monitored the laser power output. When it reached a level adequate for ignition, the computer inserted the tungsten target rod for a preset length of time (usually 0.1 s). During this time, the target was automatically retracted if the formation of a plasma was detected by a photocell positioned just below the bell jar. This system proved to be extremely reliable, and resulted in no laser-induced rod failures.

In all, over 100 separate laser thruster test firings were conducted using argon and hydrogen propellants, with each test lasting 1–2 min. Figure 7 is a typical photograph of a laser-sustained plasma within the thruster during operation. The plasma is inside the quartz cylinder and cone at the center of the photograph (the threaded rods are bolts attached to the throat section). Plasma sizes were in good agreement with pretest predictions and earlier experimental data. Both photographs and videotapes were taken during the tests. The

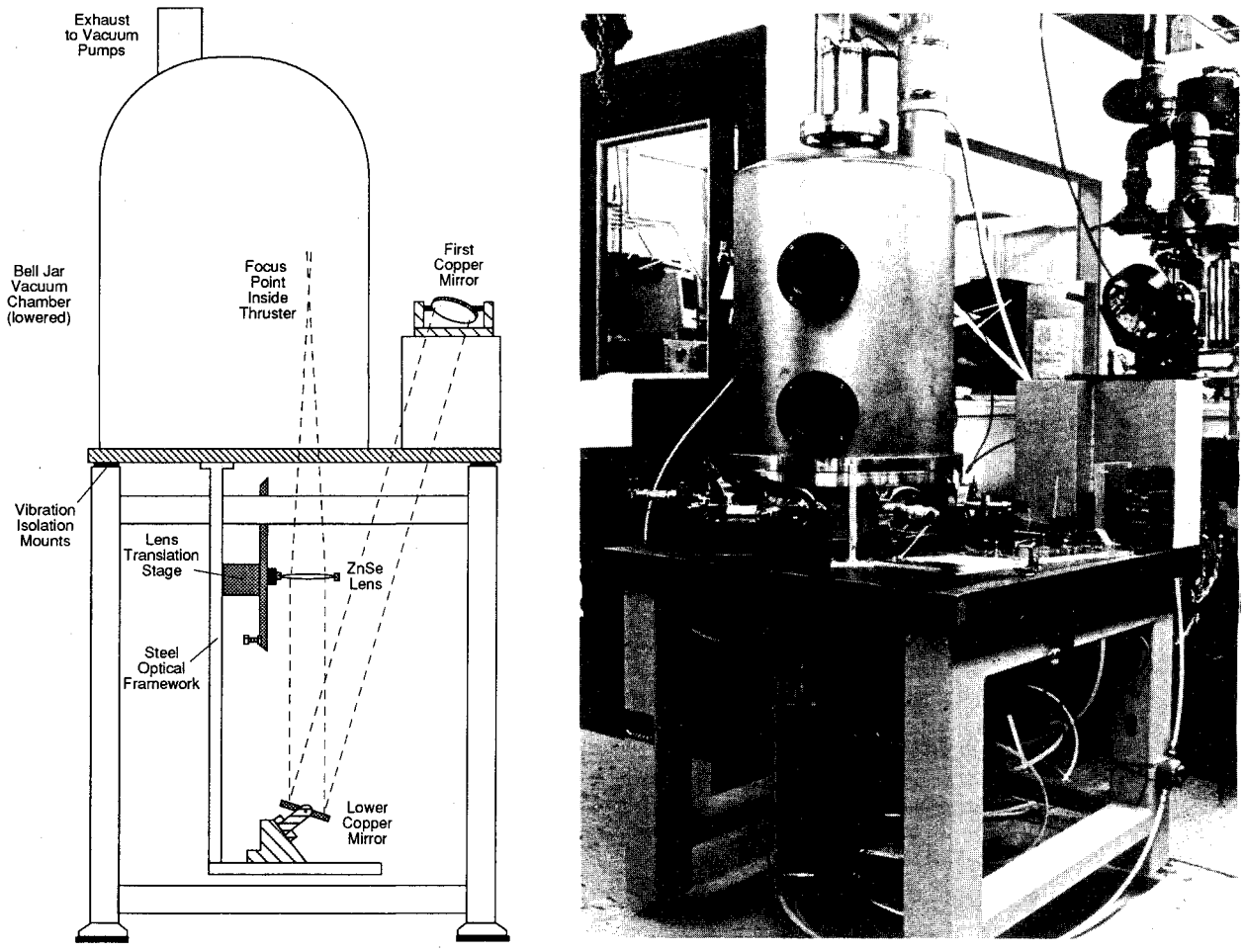

Fig. 6 Design drawing (left) and photograph (right) of laser thruster test stand with laser-focusing optics.

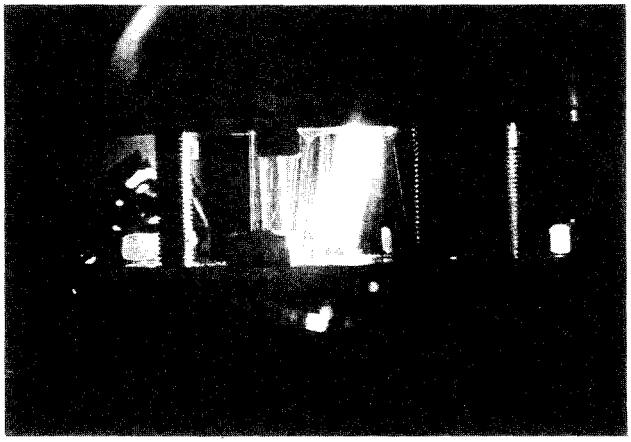

Fig. 7 Photograph of hydrogen laser-sustained plasma inside thruster during operation.

videotapes proved useful in diagnosing plasma instabilities that occurred during some tests.

Calibration Procedures and Estimated Errors

Detailed calibrations were performed for all of the diagnostic systems, especially those used in determining the thrust output and mass flow rate input, since these are used to calculate specific impulse and efficiency values. All flow meters were periodically calibrated using a laboratory-standard vibrating reed flow meter, with overall errors for both argon and hydrogen estimated at 4%. Laser power was calibrated periodically throughout the tests, with a resultant measurement accuracy of 5%. The thrust measurement system was fully calibrated before and after each test using weights dropped on the thruster. No detectable shift in the calibration was observed, and total thrust measurement errors were estimated at 2% under worst-case conditions. The accuracy of our reported specific impulse values is about 6% (worst case) for both the argon and hydrogen tests. Efficiency accuracies are about 14% (worst case).

Argon Thruster Results

Test conditions and data from thruster tests using argon propellant are summarized in Table 1. In this table, configuration 1 refers to the 5.0-mm copper throat section with a 19-deg wall angle, and configuration 2 refers to the 8-deg throat section. LSP position refers to the location of the plasma in terms of motor steps, where 3870 is the starter rod location and the motor scale factor is 787 steps/cm. The measured laser power, mass flow rate, and thrust output shown in Table 1 were used to calculate the specific impulse and efficiency performance. The following relation is used to calculate specific impulse:

$$I_{sp}(\text{s}) = F\ (\text{N})/[\dot{m}\ (\text{kg/s}) \cdot 9.8\ \text{m/s}^2] \qquad (1)$$

where I_{sp} is the specific impulse, $\dot{m}$ is the mass flow rate, and F is the thrust output. Efficiency is calculated from the relation:

$$\eta = F^2/2\dot{m}P_L \qquad (2)$$

where P_L is input laser power at the thruster entry window.

Figure 8 plots specific impulse vs thruster pressure for the 5.0-mm diam throat section. The lines connecting the data

Table 1 Test conditions for argon thruster operation

Test number	Test date	Configuration number	Laser power, W	LSP position, steps	Pressure (cold), psia	Pressure (hot), psia	Mass flow rate (hot), g/s	Thrust (hot), lbf	Calculated I_{sp}, s	Calculated efficiency	Notes
A1	7/15	1	5500	6000	13.9	22.5	6.1	1.09	81.2	0.24	2-min run; lower oil seal damaged
A2	7/15	1	5500	6000	18.0	27.0	7.9	1.24	71.1	0.20	Switch to 30-s nominal run time
A3	7/15	1	5500	6000	22.0	31.1	9.2	1.36	67.1	0.19	
A4	7/15	1	7000	6000	22.7	34.5	9.4	1.51	72.8	0.20	
A5	7/15	1	7000	6000	19.9	29.0	7.9	1.36	78.0	0.21	
A6	7/15	1	7000	6000	16.9	25.3	6.7	1.21	81.5	0.21	Steel cone discoloration
A7	7/16	1	7000	6000	15.0	24.4	6.2	1.15	84.4	0.21	
A8	7/16	1	7560	6000	21.0	31.9	8.3	1.42	77.4	0.20	
A9	7/16	1	7000	6500	20.7	31.0	8.3	1.37	74.5	0.19	
A10	7/16	1	7000	7000	20.6	31.0	8.3	1.36	74.2	0.19	
A11	7/16	1	7000	7300	20.3	32.0	8.5	1.39	74.2	0.19	Steel cone meltage found
A12	7/17	2	7000	7000	23.5	37.4	9.2	1.56	76.2	0.23	
A13	7/17	2	7000	7000	23.7	36.8	9.2	1.54	75.5	0.22	Early laser shutdown
A14	7/17	2	7000	7000	20.4	31.7	7.9	1.33	76.2	0.20	
A15	7/17	2	7000	7000	17.4	27.5	6.7	1.17	79.1	0.19	
A16	7/17	2	7000	7000	15.2	25.2	5.7	1.12	88.3	0.22	
A17	7/18	2	7000	6500	20.6	33.3	7.7	1.37	80.9	0.23	
A18	7/18	2	7000	7500	19.8	32.0	7.5	1.31	79.7	0.21	Cold pressure reduction needed for ignition
A19	7/18	2	7000	8000	19.7	31.2	7.5	1.32	79.4	0.21	
A20	7/18	2	7000	8500	—	—	—	—	—	—	Laser shutdown before reaching run position
A21	7/18	2	7000	8500	19.5	31.1	7.3	1.28	79.3	0.21	Blowout just as plasma reached run position
A22	7/18	2	7000	7000	15.5	26.0	5.9	1.07	81.7	0.18	Laser shutdown early in run
A23	7/18	2	7000	7000	15.4	25.4	6.0	1.11	82.8	0.19	
A24	7/18	2	7000	7000	13.1	23.3	5.1	1.04	92.8	0.22	New wide-body steel cone used

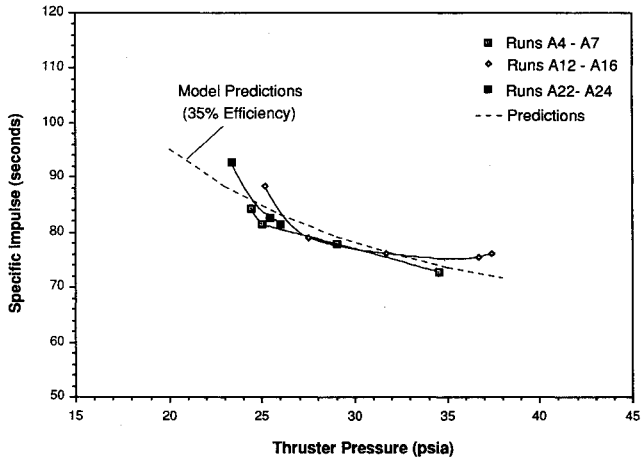

Fig. 8 Specific impulse vs pressure for argon, compared to predicted performance.

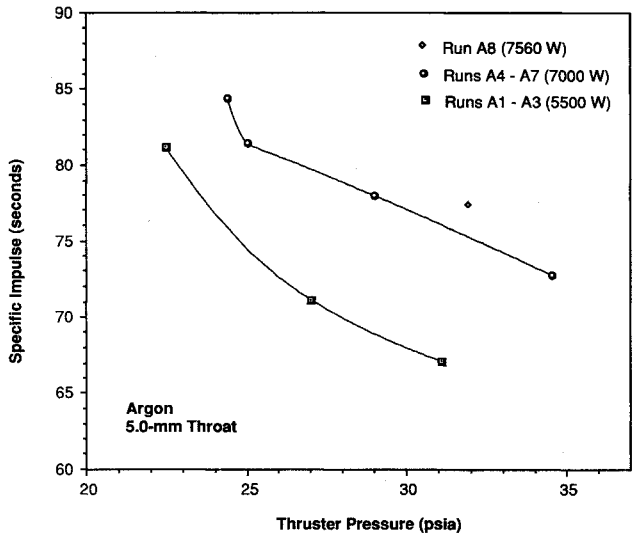

Fig. 9 Impacts of laser power on specific impulse for argon propellant.

points indicate that the runs were taken in sequence; thus, the data are most directly comparable. Specific impulse rises as the thruster pressure is reduced, since the mass flow rate decreases, creating a large rise in stagnation temperature and increased specific impulse performance. These results are in very good agreement with the results of a simulation developed to predict the performance of the thruster, shown as the dashed line in Fig. 8 (using a plasma conversion efficiency assumption of 35% based on previous test data[2]).

The effect of laser power on specific impulse is shown in Fig. 9. As the laser power increases, gas temperatures rise, causing an increase in specific impulse. The two curves show data for laser powers of 5500 and 7000 W, plus a single data point taken at 7560 W. All of this data was taken using the larger 5.0-mm throat, which accounts for the low specific impulse values (<100 s). As the throat size is reduced, the mass flow through the thruster decreases, and propellant temperatures increase. Figure 10 plots specific impulse of the 5.0-mm throat compared to the smaller 3.0-mm throat, as a function of thruster pressure. As expected, specific impulse values are significantly higher for the 3.0-mm throat, approaching 200 s at lower operating pressures.

The efficiency of the thruster was also determined for each run, with typical results in the 20–25% range, which is consistent with pretest predictions. Figure 11 plots the efficiency data vs specific impulse, indicating that there is a trend towards higher efficiency as the specific impulse increases. This is somewhat surprising, since it was anticipated that under high specific impulse operating conditions, the higher gas temperatures would lead to increased thermal losses and a re-

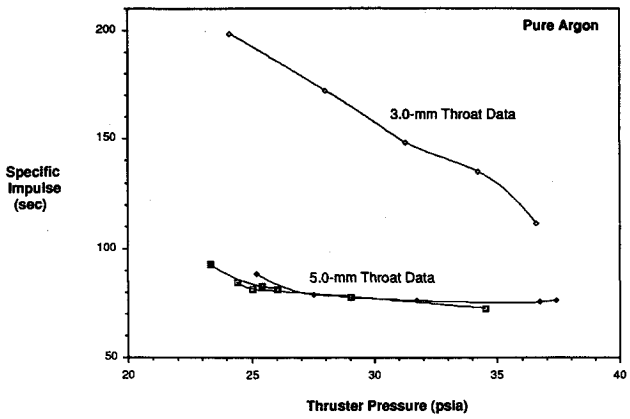

Fig. 10 Performance comparison between 3.0- and 5.0-mm throat sections.

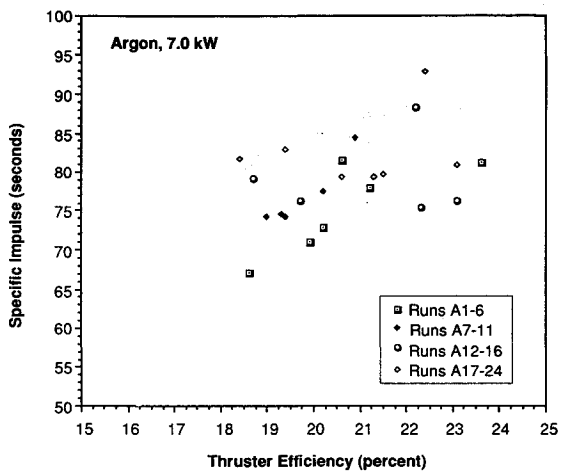

Fig. 11 Specific impulse vs efficiency data using argon propellant.

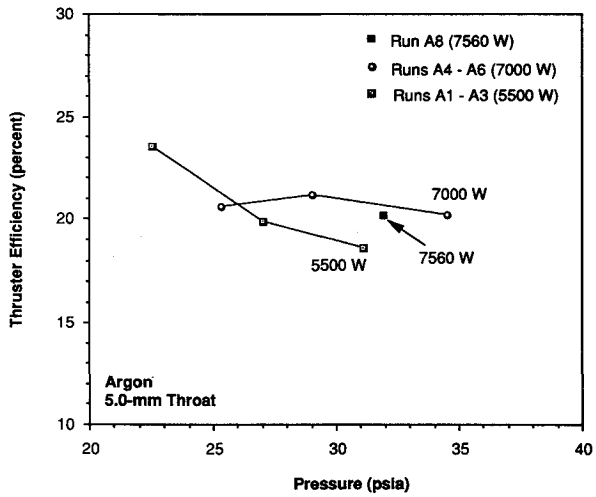

Fig. 12 Efficiency vs laser power for argon propellant.

duction in efficiency. An additional set of data suggests that as the laser power is increased, the efficiency tends to increase slightly, as shown in Fig. 12. However, the difference is within the experimental error of the data, and there are insufficient data points to establish a clear trend. But this type of trend would be consistent with plasma modeling predictions, which indicate that efficiency should increase as a weak function of laser power, due to improved plasma absorption as the laser power is raised.

Argon/Hydrogen Mixture Tests

Because hydrogen plasmas tend to be more difficult to ignite than argon plasmas (due to the loss of electron energy to vibrational molecular energy and hydrogen dissociation), a gradual method of initiating hydrogen plasmas was attempted first; namely, igniting a plasma in pure argon, then gradually transitioning from argon to hydrogen while maintaining a stable plasma. Although conceptually straightforward, this process was not successful in producing pure hydrogen plasmas, largely because of difficulties in achieving a smooth shutdown of the argon flow using a manually activated valve (the resultant flow instabilities usually caused the plasmas to prematurely extinguish). Some data for thruster specific impulse and efficiency as a function of hydrogen concentration were taken, but it was concluded that this technique for initiating hydrogen plasmas was unreliable, at least using the available equipment.

Hydrogen Plasma Stability Mapping Experiments

Following the mixture tests, our first attempts to initiate plasmas in pure hydrogen proved unsuccessful, despite trials over a broad pressure range using different throat configurations. Typically, a plasma would briefly form when the starter rod was inserted, but within a few seconds after retracting the rod, the plasma extinguished. Videotape data indicated that the plasmas appeared to be extinguishing due to a "low-end blowout" phenomenon; i.e., the flow rate through the plasma appeared to be too low to stably sustain a plasma, and at the moment of extinguishment, the plasma moved rapidly upstream.

Since this type of low-end blowout process had never been observed before, it was decided to conduct a series of plasma stability tests using a plasma chamber. Stability data was collected at a 7.0-kW power level and *f*/8.5 focusing optics. For each series of tests, a fixed chamber pressure was used, but with different flow rates established for each run. The laser would then be turned on and plasma initiation attempted. This procedure allowed us to accurately define both the high-end blowout limit, and also a newly discovered low-end blowout limit for hydrogen plasmas.

The results of these tests are summarized in Fig. 13, which plots all cases that produced stable hydrogen plasmas. We have also included several other data points taken using *f*/7 focusing optics. As the data indicates, very definite low- and high-end blowout limits were found. Even more interesting is the fact that the stable region shrinks with decreasing pressure and completely vanishes at a pressure of about 25 psia. This immediately showed why previous efforts to ignite pure

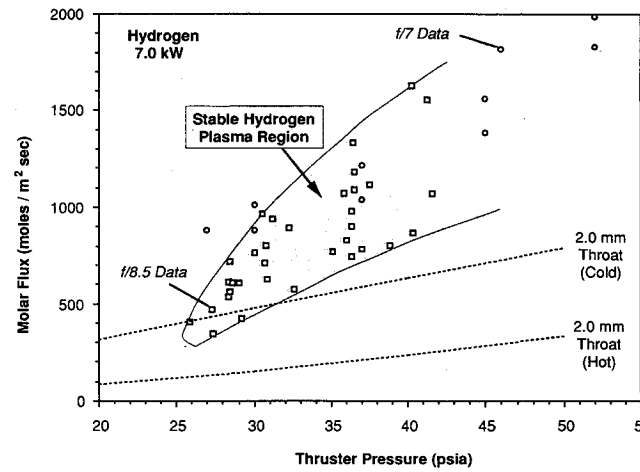

Fig. 13 Measured region of plasma stability for hydrogen LSPs. Shaded region outlines stable data points. Lines are operating conditions of thruster when using 2.0-mm throat section.

hydrogen plasmas had failed, since most of the ignition attempts were made at pressures below 30 psia.

The ignition problem may be more clearly understood by overlaying flow rates from the different nozzle geometries. For example, the dashed lines in Fig. 13 show the molar mass flux through the 2.0-mm throat section at the location of the starter rod. During cold operation, the mass flow rate is a direct function of thruster pressure, following the line labeled "Cold" in the figure. After ignition, the increased propellant temperature reduces the mass flow rate, and the thruster operates on the line labeled "Hot." In order to achieve successful ignition, it appears that the mass fluxes must lie in the stable region both before and after ignition. Obviously, for the 2.0-mm throat, both the cold and hot conditions were far below the low-end blowout limits for the plasma, preventing the formation of a stable plasma.

Overlaying flow rates for the 3.0-mm throat (Fig. 14) reveals a more stable situation, since both the hot and cold flow lines lie within the stable plasma region. Thus, when the 3.0-mm throat was used at an initial pressure of 35 psia, pure hydrogen plasmas were immediately ignited and stably maintained (note that we also increased the laser power for ignition from 7.0 to 8.2 kW, since previous test experience suggested that the stability limits are broadened as the laser power is raised).

The ignition process typically resulted in an immediate rise in thruster pressure (to nearly 50 psia) following plasma ignition, as shown by the arrow connecting points 1 and 2 in Fig. 14. This sudden pressure rise is caused by the sudden deposition of laser energy. Since these high thruster pressures typically produced poor specific impulse performance, attempts were then made to reduce the pressure to levels near 30–35 psia. This procedure involved moving the plasma upwards to raise the mass flux incident at the plasma, so as to keep the plasma away from the low-end blowout limit at point "2." This corresponds to moving from point 2 to point "3" in Fig. 14. We would then attempt to reduce the thruster pressure. However, the plasmas usually extinguished during this process, apparently due to an inability to gradually adjust the hydrogen mass flow rate using a manually controlled valve. A shortage of laser test time prevented us from correcting this problem and acquiring test data at lower thruster pressure levels.

While the plasma stability map was being defined, we were also able to simultaneously collect data on the conversion efficiency of the hydrogen plasmas whenever a stable plasma was formed. Plasma conversion efficiencies near 60% were observed at mass fluxes similar to those found in the laser thruster.

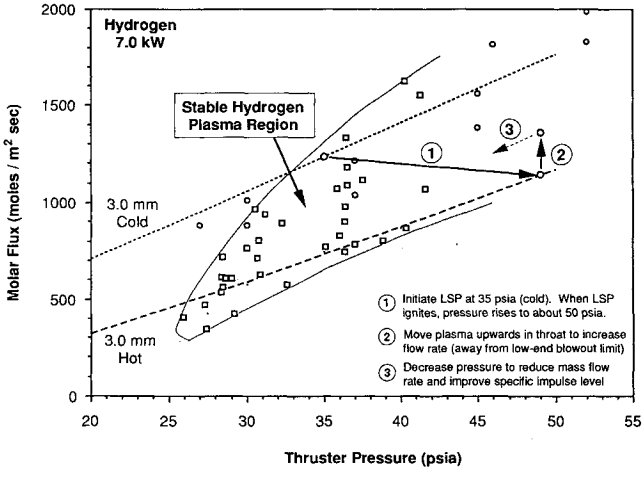

Fig. 14 Startup procedure using the 3.0-mm throat section. Initial pressure rise (1) is caused by sudden deposition of laser energy.

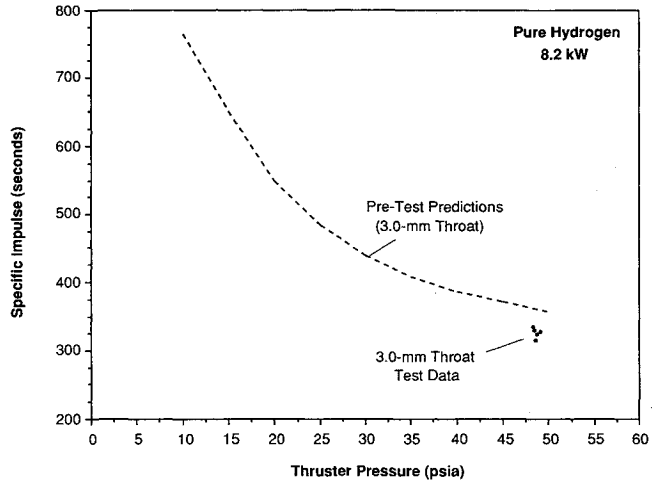

Fig. 15 Specific impulse data for hydrogen propellant using 3.0-mm throat section. Curve indicates predicted performance as a function of thruster pressure.

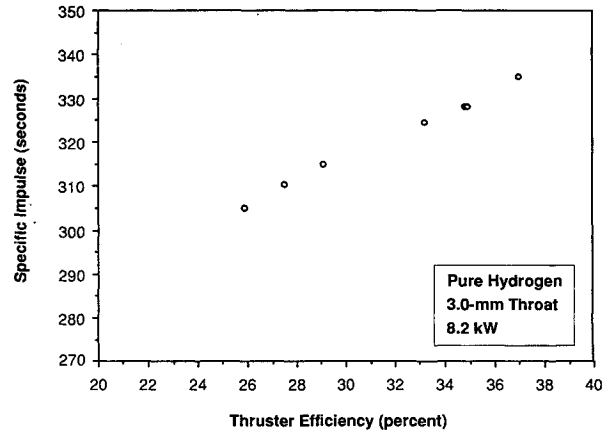

Fig. 16 Specific impulse vs efficiency using hydrogen propellant.

Hydrogen Thruster Results

Test conditions for runs utilizing pure hydrogen propellant are summarized in Table 2. After successful ignition of the hydrogen plasmas, the specific impulse data shown in Fig. 15 were collected (with values in the range of 310–340 s). Because of plasma stability limits, data were only collected for thruster pressures near 50 psia. Thus, demonstrations of the higher performance levels at lower thruster pressures (as illustrated by the prediction curve shown in Fig. 15) were not conducted. Plasma stability limits also prevented operation of the thruster using the higher-performance 2.0-mm throat, which was expected to produce specific impulse levels of up to 700 s. Modifications to the 2.0-mm thruster hardware that would place the plasma within the stable region were identified, but there was insufficient test time available to implement these changes.

Hydrogen-efficiency data were also collected, as shown in Fig. 16. This plot again shows a trend of increased efficiency as specific impulse is raised. Typical efficiencies for the hydrogen tests were in the range of 25–40%, slightly lower than the pretest predictions of 35–45%. The data suggest that a sizable portion (probably about one-third) of the laser energy absorbed by the plasma in the thruster is being lost as thermal heat to the nozzle walls.

100-kW Thruster Design

The ultimate objective of laser propulsion testing is to demonstrate the operation of a laser thruster at power levels more

Table 2 Test conditions for pure hydrogen operation

Test number	Configuration number	Laser power, W	LSP position, steps	Pressure (cold), psia	Pressure (hot), psia	Mass flow H_2 (hot), g/s	Thrust (hot), lbf	Calculated I_{sp}, s	Calculated efficiency	Notes
H1	3	7000	3870	32.4	—	—	—	—	—	No plasma ignition
H2	3	7000	3870	35.0	—	—	—	—	—	No plasma ignition
H3	3	7000	3870	37.6	—	—	—	—	—	No plasma ignition
H4	3	7000	3870	40.2	—	—	—	—	—	No plasma ignition
H5	3	7000	3870	30.2	—	—	—	—	—	No plasma ignition
H6	3	7000	3870	27.8	—	—	—	—	—	No plasma ignition
H7	3	5500	3870	35.0	—	—	—	—	—	No plasma ignition
H8	3	8200	3870	35.0	—	—	—	—	—	5-s plasma, then laser shut down
H9	3	8200	3870	35.2	—	—	—	—	—	5-s plasma, then laser shut down
H10	3	8200	3870	35.1	—	—	—	—	—	3-s plasma, then plasma extinguished
H11	3	8200	3870	35.1	—	—	—	—	—	Plasma blew out when lens motion started
H12	3	8200	3870	35.0	48.9	1.133	0.762	304.7	0.259	Plasma blew out after about 11 s
H13	3	8200	4760	35.0	47.9	1.128	—	—	—	Plasma blew out at about 890 steps up
H14	3	8200	4815	35.0	48.3	1.133	—	—	—	Lens moved at half-speed, plasma blew out at 945 steps
H15	3	8200	3870	35.0	—	—	—	—	—	No plasma ignition
H16	3	8200	4320	35.0	48.8	1.125	—	—	—	No thrust data–incorrect counterweight used Plasma held for 25 s, then laser shut down
H17	3	8200	4320	34.9	44.8	—	0.692	—	—	No mass flow data—pressure gauge out of limits
H18	3	8200	4320	35.0	46.6	0.856	—	—	—	Plasma blew out after several seconds
H19	3	8200	4320	35.1	48.8	1.103	—	—	—	Plasma blew out on way up to 4320
H20	3	8200	4320	35.0	48.3	1.088	0.8033	334.5	0.370	20-s nominal test run time used
H21	3	8200	4550	35.2	49.2	1.108	0.8022	328.0	0.349	
H22	3	8200	4700	35.3	48.5	1.104	0.7997	328.2	0.348	Laser shutdown after 15 s
H23	3	8200	4850	35.3	48.5	1.101	0.7647	314.7	0.291	
H24	3	8200	5000	35.3	48.7	1.101	0.7884	324.4	0.332	
H25	3	8200	5150	35.3	48.4	1.104	0.7567	310.5	0.275	Plasma blew out on way to 5150 (near 5000) Video shows clear high-end blowout
H26	3	8200	5000	35.3	48.4	—	0.7571	—	—	Test aborted after plasma ignition—lens motion problem
H27	3	8200	5000	35.3	47.3	—	0.7383	—	—	Hydrogen pressure dropped during run—tanks emptied
H28	3	8200	3870	35.3	47.7	—	0.712	—	—	Plasma blew out after about 3 s
H29	3	8200	4400	35.3	47.4	—	0.7007	—	—	Plasma blew out on way up to 5000
H30	3	8200	—	35.3	—	—	—	—	—	No plasma ignition, starter rod tack-welded

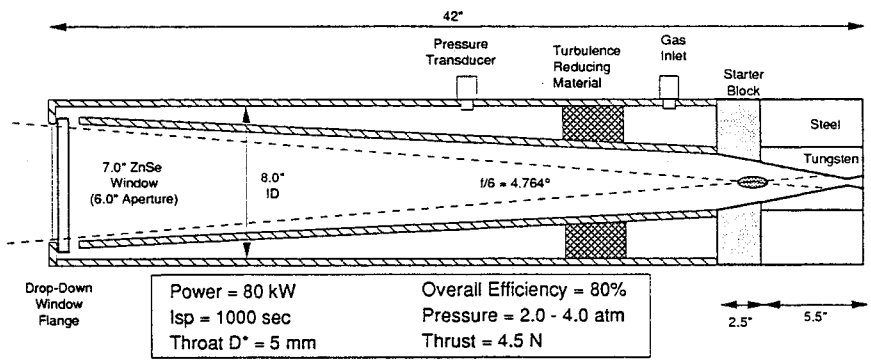

Fig. 17 Preliminary design for a 100-kW laser thruster. Predicted performance: 1000-s specific impulse, 80% conversion efficiency, 4.5-N thrust output.

typical of an operational thruster unit (100 kW to 1 MW). As an intermediate step, a design was developed for a thruster to be tested at a power level of 100 kW, as shown in Fig. 17. This design incorporates many important lessons learned during the 10-kW thruster fabrication and testing efforts, such as the use of shorter focal length focusing optics to improve plasma stability, a revised starter-rod assembly that is less prone to thermal stresses, and a revised ZnSe window flange for more rapid disassembly for window replacement. Most of the test support equipment developed for the 10-kW system is reusable for 100-kW testing with minor modifications. Preliminary performance predictions for the 100-kW thruster indicate that specific impulse levels of 1000 s should be achievable, at efficiencies of about 80%. An important remaining issue is the determination of how the low-end blowout limit scales with laser power (high-end limit scaleability is well established).

Summary and Conclusions

For the first time, it has been demonstrated that a high-power CW laser beam can be used to stably power a rocket engine. In over 100 separate laser thruster test firings, performance was accurately quantified over a broad range of operating conditions. Specific impulse values near 350 s were recorded for hydrogen, at conversion efficiencies near 40%. All of the specific impulse and conversion efficiency results were in good agreement with pretest predictions. It was also found that laser-sustained plasmas can be stably maintained in confined choked-flow environments, but that "low-end" blowout limits exist and must be considered when designing the thruster. Additional data is needed to quantify these limits at higher laser powers, and establish the physical mechanism responsible for the instability. Many of the hardware systems developed for the laser thruster tests proved to be highly successful, such as the "vertical balance" thrust measurement system with counterforce coil and LVDT, which proved to be extremely accurate yet easy to operate.

The successful completion of this program represents a major milestone in the advancement of laser propulsion technology. Future programs will now have a detailed database against which new performance models can be compared, and future experimental test programs at higher laser powers can now be more confidently planned and executed using the experience gained during these tests.

Acknowledgments

Funding for this program was provided through an SBIR Phase II award from the SDIO Office of Innovative Science and Technology. Leonard H. Caveny was the Contract Monitor. Additional technical direction was provided by David C. Byers of NASA LeRC, and the authors acknowledge the advice and assistance of many members of the NASA LeRC staff during the design of our equipment. The authors are also indebted to the University of Illinois for the use of their 10-kW laser facility.

References

[1]Kantrowitz, A., "Propulsion to Orbit by Ground-Based Lasers," *Astronautics and Aeronautics*, Vol. 10, May 1972, pp. 74–76.

[2]Schwartz, S., Mertogul, A., Eguiguren, J., Zerkle, D., Chen, X., Krier, H., and Mazumder, J., "Laser-Sustained Gas Plasmas for Application to Rocket Propulsion," AIAA Paper 89-2631, July 1989.

[3]Welle, R., Keefer, D., and C. Peters, "Energy Conversion Efficiency in High-Flow Laser-Sustained Argon Plasmas," AIAA Paper 86-1077, May 1986.

[4]Black, J. W., Cowie, R. C., Glumb, R. J., and Krier, H., "10-kW Laser Propulsion Thruster Test Program Final Report," CSI TR CSI-91-03, NASA CR-189119, Dec. 1991.